Clim. Past Discuss., 11, 4943–4984, 2015
www.clim-past-discuss.net/11/4943/2015/
doi:10.5194/cpd-11-4943-2015

Climate of the Past
Discussions
Open Access

Frequency and intensity of palaeofloods at the interface of Atlantic and Mediterranean climate domains

B. Wilhelm[1,2], H. Vogel[2], C. Crouzet[3,4], D. Etienne[5], and F. S. Anselmetti[2]

[1]Univ. Grenoble Alpes, LTHE, 38000 Grenoble, France
[2]Institute of Geological Sciences and Oeschger Centre for Climate Change Research, Univ. of Bern, 3012 Bern, Switzerland
[3]Univ. Savoie Mont Blanc, ISTerre, 73376 Le Bourget-du-Lac, France
[4]CNRS, ISTerre, 73376 Le Bourget-du-Lac, France
[5]UMR INRA 42 CARRTEL, Univ. Savoie Mont Blanc, 73376 Le Bourget du Lac, France

Received: 22 September 2015 – Accepted: 3 October 2015 – Published: 23 October 2015

Correspondence to: B. Wilhelm (bruno.wilhelm@ujf-grenoble.fr)

Published by Copernicus Publications on behalf of the European Geosciences Union.

Abstract

The long-term response of the flood activity to both Atlantic and Mediterranean climatic influences was explored by studying a lake sequence (Lake Foréant) of the Western European Alps. High-resolution sedimentological and geochemical analysis revealed 171 turbidites, 168 of which result from past flood events over the last millennium. The deposit thickness was used as a proxy of intensity of past floods. Because the Foréant palaeoflood record is in agreement with the documented variability of historical floods resulting from local and mesoscale convective events, it is assumed to highlight changes in flood frequency and intensity related to such events typical of both climatic influences. Comparing the Foréant record with other Atlantic-influenced and Mediterranean-influenced regional flood records highlights a common feature in all flood patterns that is a higher flood frequency during the cold period of the Little Ice Age (LIA). In contrast, high-intensity flood events are apparent during both, the cold LIA and the warm Medieval Climate Anomaly (MCA). However, there is a tendency towards higher frequencies of these events during the warm MCA. The MCA extremes could mean that under the global warming scenario, we might see an increase in intensity (not in frequency). However, the flood frequency and intensity in course of 20th century warming trend did not change significantly. Uncertainties lie in the interpretation of the lack of 20th century extremes (transition or stable?) and the different climate forcing factors (greenhouse gases vs. solar/volcanic eruptions).

1 Introduction

Heavy rainfall events trigger mountain-river floods, one of the most significant natural hazards, causing widespread loss of life, damage to infrastructure and economic deprivation (e.g. Münich Re Group, 2003). This is especially the case for the Alpine area in Europe, where tourism and recent demographic development with an increasing population raise the vulnerability of infrastructure to natural hazards (e.g. Beniston and Stephenson, 2004). Moreover, the current global warming is expected to trigger an intensification of the hydrological cycle and a modification of flood hazard (IPCC et al., 2013). Hence, a robust assessment of the future evolution of the flood hazard over the Alps becomes a crucial issue.

A main limitation for robust flood-hazard projections is the scarce knowledge on the underlying natural climate dynamics that lead to these extreme events (IPCC, 2013). Indeed, the stochastic nature and the rare occurrence of extreme events make the identification of trends based on instrumental data alone difficult (e.g. Lionello et al., 2012). One way of overcoming this issue is to extend flood series beyond observational data and compare these datasets with independent climatic and environmental forcing. In this purpose, many types of sedimentary archives have been studied (e.g. Luterbacher et al., 2012 and references therein). Among them lake sediments are being increasingly studied because they allow to reconstruct flood records long enough to identify the natural variability at different time scales (e.g. Noren et al., 2002; Oslegger et al., 2009; Wilhelm et al., 2012a; Czymzik et al., 2013; Glur et al., 2013; Corella et al., 2014).

In the western Alps, many lake-sediment sequences have been studied to better assess the response of the flood activity to the climate variability. These studies revealed higher flood frequency of mountain streams in many regions during multi-centennial cold phases such as the Little Ice Age (Giguet-Covex et al., 2012; Wilhelm et al., 2012a, 2013; Glur et al., 2013; Wirth et al., 2013b; Amann et al., 2015). However, regarding flood intensity/magnitude, opposite patterns appear with the occurrence of the most extreme events during warmer periods in the north (Giguet-Covex et al., 2012; Wilhelm et al., 2012b, 2013), while they occurred during colder periods in the south (Wilhelm et al., 2012a, 2015). These north–south opposite flood patterns were explained by flood-triggering meteorological processes specific to distinct climatic influences: atlantic in the north Mediterranean in the south. In the north-western part, floods at high altitude are mainly triggered by local convective events (i.e. thunderstorms) and seem to mainly depend on the temperature that would strengthen vertical

CPD
11, 4943–4984, 2015

processes (e.g. Wilhelm et al., 2012b, 2013). In contrast, floods in the south are mostly triggered by mesoscale events and may strongly depend on changes in atmospheric circulations, i.e. their pathways and intensity (e.g. Boroneant et al., 2006; Boudevillain et al., 2009). By analogy with these results over past warm periods, the mountain-flood hazard might be expected to increase in the north-western Alps, mainly because of an enhanced flood magnitude associated to stronger convective processes. Hence, better assessing the spatial extent of the Atlantic-influenced flood pattern at high-altitude appears a crucial issue to appropriately establish hazard mitigation plans and prevent high socio-economic damages.

In this frame, the present study was designed to reconstruct the flood pattern at an intermediate situation between the north-western and south-western Alps, i.e. at the climate boundary between Atlantic and Mediterranean influences. This is undertaken by reconstructing a millennium-long flood chronicle from the sediment sequence of the high-altitude Lake Foréant located in the Queyras massif.

2 Regional setting

2.1 Climate and historical flood

The Queyras massif is located in between the northern and southern French Alps where the climate is influenced by the Atlantic Ocean and the Mediterranean Sea (Fig. 1). As a result, the Queyras mountain range corresponds to a transition zone of Alpine precipitation patterns in the meteorological reanalyses (Durant et al., 2009; Plaut et al., 2009) and in the simulations (Frei et al., 2006; Rajczak et al., 2013). In the Queyras, heavy precipitation events are related to either local convective phenomena (i.e. summer thunderstorms) or mesoscale convective systems. The mesoscale systems called “Lombarde-Type” or “East Return” events occur mainly from late spring to fall and result from Mediterranean humid air masses flowing northward into the Po Plain and then westward until the Queyras massif (e.g. Gottardi et al., 2010; Parajka et al., 2010). The humid air masses are then vigorously uplifted with the steep topography of the Queyras massif, causing an abrupt cooling of the air masses and intense precipitations. Such mesoscale precipitation events, typical of the Mediterranean climate (e.g. Buzzi and Foschini, 2000; Lionello et al., 2012), affect extensive areas and may lead to catastrophic floods at a regional scale as shown in June 1957 or October 2000 over the Queyras massif (Arnaud-Fassetta and Fort, 2004). Other numerous past flood events have been documented from studies of local historical records. These data have been compiled in a database managed by the ONF-RTM (http://rtm-onf.ifn.fr/). They show that the village of Ristolas (located 8 km downstream from Lake Foréant, Fig. 1c) has been affected at least 34 times over the last 250 years by floods of the Guil River and its five main tributaries (see Supplement).

2.2 Lake Foréant and its tributaries

Lake Foréant (2620 m a.s.l., 44°42′20″ N, 6°59′00″ E) is located in a cirque of 3 km^2 in the upper part of the Queyras Massif, adjacent to the Italian border (Fig. 1). It is located approximately 60 km north from Lake Allos and 100 km south-west from Lakes Blanc, where the south-western and north-western flood patterns have been shown (Wilhelm et al., 2012a, b; Fig. 1b). The catchment rises up to 3210 m. a.s.l. and is made up of three lithologies from the Queyras schistes-lustrés nappe (e.g. Schwartz et al., 2009), (i) marble in the eastern part, (ii) calc-schist in the western part and (iii) a narrow band of arkose in between (Fig. 1d). The main stream of the catchment, the Torrent de Bouchouse, drains mainly the central band of arkose. Before entering the lake, this stream has built a fluvial plain where it is divided in two meandering branches (Fig. 1e). This suggests that the Bouchouse stream is a major source of sediment entering the lake. In addition, two minor and non-permanent streams drain the western part of the catchment. In contrast, they enter the lake through small deltas, suggesting limited detrital inputs. There is no evidence of glacial deposits in the catchment and, thereby, detrital inputs only result from the erosion and transport of these lithologies. Detrital inputs from these streams are limited to summer and fall because the catchment is covered

CPD
11, 4943–4984, 2015

by snow and the lake is frozen from mid-November to the beginning of June. The Bouchouse stream flows downstream into the Guil River and reaches approximately 8 km further the village of Ristolas (Fig. 1c).

3 Method

3.1 Lake coring

In summer 2013, a bathymetric survey was carried out on Lake Foréant and revealed a well-developed flat basin in the centre of the lake with a maximum water depth of 23.5 m (Fig. 1e). An UWITEC gravity corer has been used to retrieve four cores along a north–south transect in the axis of the two main inlets. Cores FOR13P3 and FOR13P4 correspond to the proximal locations of the two different branches of the Bouchouse stream and aim at investigating their respective sediment inputs during floods. Cores FOR13P2 and FOR13P1 correspond to the depocenter and to the most distal position, i.e. the opposite slope to the Bouchouse inflows, respectively.

3.2 Core description and logging

Cores were split lengthwise and the visual macroscopic features of each core were examined to identify the different sedimentary lithofacies. The stratigraphic correlation between the cores was then carried out based on these defined lithofacies.

High-resolution color linescans and gamma-ray attenuation bulk density measurements were carried out on a GeotekTM multisensor core-logger (Institute of Geological Sciences, University of Bern). Bulk density was used as a proxy of event layers, e.g. flood deposits, characterized by higher density due to the high amount of detrital material deposited in a short time (e.g. Støren et al., 2010; Gilli et al., 2012; Wilhelm et al., 2012b).

Grain size analyses on core FOR13P2 were performed using a Malvern Mastersizer 2000 (Institute of Geography, University of Bern) on sub-samples collected at a 5 mm

CPD
11, 4943–4984, 2015

continuous interval. Before grain-size analysis, the samples were treated in a bath of diluted hydrogen peroxyde during 3 days to remove organic matter. These grain-size analyses of the detrital material were performed to study the transport-deposition dynamics of the deposits (e.g. Passega, 1964) and to establish a proxy of flood intensity. Grain-size variability is assumed to represent the river energy and, thereby, the maximum discharge volume reached during the flood event (Campbell, 1998; Wilhelm et al., 2015).

Geochemical analysis and X-ray imaging were carried out using an Itrax™ (Cox Analytical Systems) X-ray fluorescence (XRF) core scanner (Institute of Geological Sciences, University of Bern), equipped with a Molybdenum tube (50 keV, 30 mA) with a 10 s count-time using sampling steps of 1 mm (XRF) and 0.2 mm (X-ray imaging). The areas of the element peaks obtained are proportional to the concentrations of each element (Tachikawa et al., 2011). Geochemical data were applied to identify flood deposits at high resolution through their higher content in detrital material (e.g. Arnaud et al., 2012; Wilhelm et al., 2012b; Czymzik et al., 2013; Swierczynski et al., 2013) and/or as high-resolution grain-size proxies (e.g. Cuven et al., 2010; Wilhelm et al., 2012a, 2013). Geochemical analyses were carried out on core FOR13P2. X-ray images highlighting the variability of the sediment density have been acquired for the four cores.

3.3 Coprophilous fungal spores analysis

Erosion processes in high-altitude catchments may be modified by grazing activity and, thereby, the climatic signal in flood reconstructions may be altered (e.g. Giguet-Covex et al., 2012). The variability of grazing pressure in a catchment area can be reconstructed from the abundance in the sediment of coprophilous fungal ascospores, i.e. *Sporormiella* (HdV-113) (e.g. Davis and Schafer, 2006; Etienne et al., 2013). To test the potential impact of grazing pressure on the reconstructed flood activity, *Sporormiella* abundance was determined in subsamples collected all along the core FOR13P3. This core was chosen because it was the sequence with the thinnest potentially-erosive event layers. During the sampling, event layers were avoided because they may correspond to turbidities related to flood or mass-movement events that may have transported unusual quantities of *Sporormiella* ascospores, or induced the remobilization of older sediments. Subsamples were chemically prepared according to the procedure of Fægri and Iversen (1989). *Lycopodium clavatum* tablets were added in each subsample (Stockmarr, 1971) to express the results in concentrations (nb cm^{-3}) and accumulation rates (nb cm^{2} yr^{-1}). Coprophilous fungal ascospores were identified based on several catalogues (Van Geel and Aptroot, 2006; Van Geel et al., 2003) and counted following the procedure established by Etienne and Jouffroy-Bapicot (2014).

3.4 Dating methods

To date the lake sequence over the last century, short-lived radionuclides (^{210}Pb, ^{137}Cs) were measured by gamma spectrometry at the EAWAG (Zürich, Switzerland). The core FOR13P4 was sampled following a non-regular step of 1 ± 0.2 cm, matching the facies boundaries. The ^{137}Cs measurements allowed two main chronostratigraphic markers to be located: the fallout of ^{137}Cs from atmospheric nuclear weapon tests culminating in AD 1963 and the fallout of ^{137}Cs from the Chernobyl accident in AD 1986 (Appleby, 1991). The decrease in excess ^{210}Pb and the Constant Flux/Constant Sedimentation (CFCS) allowed a mean sedimentation rate to be calculated (Goldberg, 1963). The standard error of the linear regression of the CFCS model was used to estimate the uncertainty of the sedimentation rate obtained by this method. The ^{137}Cs chronostratigraphic markers are then used to control the validity of the ^{210}Pb-based sedimentation rate.

To date the sequence beyond the last century, small-size vegetal macro-remains were sampled in core FOR13P4. Terrestrial plant remains were isolated at the Institute of Plant Sciences (University of Bern) and sent for AMS ^{14}C analysis to the AMS LARA Laboratory (University of Bern). ^{14}C ages were calibrated using the Intcal13 calibration curve (Reimer et al., 2013; Table 1). Using the R-code package “clam” (Blaauw,

CPD
11, 4943–4984, 2015

2010), an age-depth model was generated from the ^{210}Pb ages, the ^{14}C ages and the palaeomagnetic chronological markers.

Palaeomagnetic chronological markers can be obtained by comparing declination and inclination of the characteristic remanent magnetization (ChRM) vs. depth to known secular variations of the geomagnetic field (e.g. Barletta et al., 2010; Wilhelm et al., 2012a). Palaeomagnetic investigations were performed at the CEREGE laboratory (University Aix-Marseille) on cores FOR13P1, FOR13P2 and FOR13P4 using u-channels. The natural remanent magnetization (NRM) was progressively demagnetized using alternating field with 10, 20, 30, 40, 60, 80 and 100 mT steps. However, before comparing magnetization carried by sediments to the known secular variations, several points need to be verified: (i) the preservation of the sedimentary magnetic fabric, (ii) the stability of magnetic mineralogy and (iii) the stability of the magnetic components. Two types of laboratory remanent magnetizations were imparted to distinguish different mineralogical and grain-size fractions within the magnetic components: Isothermal Remanent Magnetization (IRM) and Anhysteretic Remanent Magnetization (ARM). ARM was produced in-line along the u-channel axis, using a 100 mT alternating field with a superimposed 0.05 mT steady field. IRM was obtained by passing the u-channels through two different Halbach cylinders that develop fields of 1 and 0.3 T (Rochette et al., 2001). For ARM and IRM1T demagnetization was done following steps of 10, 20, 30, 40, 60, 80 and 100 mT. The magnetizations have been measured before alternating-field treatment and after each step using the 3 axis 2-G enterprise cryogenic magnetometer located in a shielded room. Additionally, anisotropy of magnetic susceptibility has been measured using AGICO MFK1-FA Kappabridge (spinning specimen method) to control the preservation of the sedimentary fabric. The susceptibility ellipsoid is defined by three eigenvectors (Kmax, Kint and Kmin). The magnetic fabric is usually comparable to the sediment fabric with inclination of the Kmin close to the vertical (Borradaile, 1988; Rochette et al., 1992; Tarling and Hrouda, 1993).

CPD
11, 4943–4984, 2015

4 Results

4.1 Sedimentology

The sediment consists of a homogeneous, brown mud mainly composed of silty detrital material and aquatic organic remains (small fragments of plants and anamorphous organic matter), representing the background hemi-pelagic sedimentation. These fine grained deposits are interrupted by 171 rather coarser-grained layers, which are interpreted to represent short-term depositional events: 3 coarse-grained layers and 168 normally graded beds (Fig. 2).

The three cm-thick coarse-grained layers are present at 75 cm in core FOR13P2 and at 9 and 42 cm in core FOR13P4 (Fig. 2). They consist of small gravels and aquatic plant remains embedded in a silty matrix. The high porosity in the sediment due to the presence of gravels generates a partial loss of XRF signal, preventing a reliable geochemical characterization. X-ray images show chaotic sedimentary structures. The stratigraphic correlation revealed that two centimetres of sediment are missing below the thickest coarse-grained layer in core FOR13P4, suggesting an erosive base for this layer. Finally, every coarse-grained layer is overlain by a normally graded bed (labelled MMIT in Fig. 2 and 3).

The 171 graded beds are characterized by their higher density, a slight fining-upward trend and a thin, whitish fine-grained capping layer (Fig. 2). There is no evidence of an erosive base. According to the stratigraphic correlation, all the graded beds extend over the entire lake basin with a regular deposition pattern. Indeed, the graded bed thickness is systematically larger in cores FOR13P2 and FOR13P4, and decreases respectively in cores FOR13P1 and FOR13P3. This suggests that the southern branch of the Bouchouse stream is the main sediment input over time (Fig. 1). The grain-size of the graded beds is dominated by silt-sized grains with only small amounts of clay/fine silt present in the whitish capping layer and to coarse silt in their basal part (Fig. 2). According to their characteristics, these deposits are all interpreted as turbidites. Their origin is discussed in Sect. 5.1.

CPD
11, 4943–4984, 2015

4.2 Geochemistry

Among the core scanner output parameters, the scattered incoherent (Compton) radiation of the X-ray tube (Mo_{inc}) may vary with the sediment density (Croudace et al., 2006) and, thereby, offer a high-resolution proxy for sediment density. Mo_{inc} values were averaged at a 5 mm resolution to be compared to the density obtained at a 5 mm resolution with the gamma-ray attenuation method. A positive and significant correlation ($r = 0.85$, $p < 10^{-4}$) between the two density parameters was found and allowed using Mo_{inc} as a proxy of sediment density for identifying millimetre-scale turibidites (Fig. 3).

The variability of the well-measured elements within the turbidites was then investigated to assess (i) a high-resolution grain-size proxy and (ii) distinct sediment-turbidite sources between the littoral (i.e. mass-movement origin) and the catchment area (i.e. flood origin). The variability of relative potassium (K) contents vs. sediment depth (Fig. 3) shows increased K contents in the capping layers of the turbidites, suggesting K enrichment in the finest sediment fraction. Relative variability in silicon (Si) contents is correlated to K contents ($r = 0.77, p < 10^{-4}$). Variations in iron (Fe) contents show an opposite pattern with Fe enrichments in the basal and coarser part of the graded beds. Interestingly, Fe is the only element which elevated in coarser-grained beds. These results suggest that the Fe/K ratio may be used as a millimetre-scale proxy for relative grain-size distribution and hence for detecting millimetre-scale graded beds. However, this ratio can not be used as a flood intensity proxy because the absence of a significant variability in the grain size precludes the proxy calibration (e.g. Wilhelm et al., 2012b, 2013).

Relative Ca intensities are most of the time very low (< 900 counts), except for several sharp peaks and two well-marked excursions (> 1200 counts) at 30 and 75 cm in core FOR13P2 (Fig. 3). These two well-marked excursions correspond to the two thick turbidites (MMIT2 and 3; Fig. 2). In addition, manganese (Mn) contents also vary within a low value range ($< 10^4$ counts) interrupted by sharp, well-marked peaks (up

CPD
11, 4943–4984, 2015

to 4.10^4 counts). All those Mn peaks are located at the base of turbidites. However not every turbidite base corresponds to a Mn peak. To better assess the relationships between those elements, the Ca contents were plotted against Fe, K and Mn contents (Fig. 4). These plots clearly highlight two groups of deposits. The background sediments and most of the turbidites (those labelled FIT in Fig. 4) are characterized by (i) low Ca contents and (ii) a high variability in Mn content. The three turbidites overlying the coarse-grained layers (those labelled MMIT in Fig. 4) show a distinct geochemical pattern with (i) a high Ca content regardless of Fe and K contents and (ii) a very low Mn content.

4.3 Chronology

The down-core ^{210}Pb excess profile for core FOR13P2 shows a continuous decrease to low values (~ 50 Bq.Kg^{-1}), punctuated by sharp excursions to low values for three layers (2–3.5 cm, 7.5–10.5 cm and 15–17 cm) corresponding to graded turbidites (Fig. 4a). In line with Arnaud et al. (2002), these values were excluded to build a corrected sedimentary record without event layers (Fig. 4b). The CFCS model (Goldberg, 1963), applied on the event-free ^{210}Pb excess profile, provides a mean sedimentation rate of 1.3 ± 0.1 mm yr^{-1} (without the event layers). Ages derived from the CFCS model were transposed to the original sediment sequence to provide a continuous age-depth relationship (Fig. 4c). The event-free ^{137}Cs profile indicated two peaks at 3.5 and 5.5 cm (Fig. 4b), interpreted as the result of the Chernobyl accident in AD 1986 and the maximum fallout of the nuclear weapon tests in AD 1963. These independent chronological markers are in good agreement with the ^{210}Pb excess ages, supporting the age-depth model over the last century (Fig. 4c).

Results of Anisotropy of Magnetic Susceptibility for core FOR13P4 show a well preserved sedimentary fabric, i.e. Kmin inclination close to the vertical, except in the thickest event layers (labelled MMIT2 and MMIT3, Fig. 2) were the Kmin inclination is clearly deviated (Fig. S1 in the Supplement). For the 3 cores, the mean destructive field of

ARM and IRM is very similar (between 20 and 30 mT) indicating a magnetic mineralogy mainly composed of low coercivity phase. The *S* ratio (Bloemendal et al., 1992) is always between 0,86 and 0,95 indicating lower coercivity and a ferrimagnetic mineralogy. This suggests a good stability of the magnetic mineralogy, except in event layers where other parameters such as the relative palaeointensity (calculated as NRM intensity divided by ARM intensity) are clearly different, highlighting a different magnetic mineralogy. PCA have then been performed using puffin plot software (Lurcock and Wilson, 2012) to calculate the ChRM. A careful examination of demagnetization diagrams shows a unidirectional behaviour (Fig. S2 in the Supplement). The Mean Angular Deviation (MAD) is usually lower than 6 revealing a good stability of the magnetization direction. In most cases, the calculated component is not straight to the origin. This is particularly the case in the event layers. This implies the occurrence of a high coercivity component of unknown origin. All cores show quite large variations of the declination and inclination vs. depth. Because of the deviation of the Kmin and changes in magnetic mineralogy, measurements from the thickest event layers (i.e. MMIT2 and MMIT3) have been removed to build event-free declination and inclination signals (Fig. 5a). Based on the stratigraphic correlation, the event-free palaeomagnetic profiles obtained for each core were all corrected to a reference depth, i.e. the event-free depth of core FOR13P2 (Fig. 5b). Finally, all magnetic profiles were averaged to obtain unique curves of declination vs. depth and inclination vs. depth (Fig. 5c), smoothing small artefacts and making it easier for comparison to the reference curve (ARCH3.4k model; Donadini et al., 2009; Korte et al., 2009). From the variations of the reference curve over the last millennium, magnetic declination minima and maxima can be identified at AD 1810±20, 1540 ± 70 and 1365 ± 25 (D-1 to D-3, respectively). For the inclination, two tie points at AD 1700 ± 30 and 1330 ± 40 can be used (I-1 and I-2, Fig. 5d). Furthermore the ChRM declination (inclination) profile presents 3 (2) declination (inclination) features over this period allowing the correlation proposed (Fig. 5). These well-correlated declination and inclination features can thus be used as additional chronological markers.

CPD
11, 4943–4984, 2015

The ^{210}Pb and the ^{14}C ages (Fig. 4 and Table 1) were then combined with the palaeomagnetic chronomarkers (Fig. 5) to construct an age-depth model covering the whole sequence (Fig. 6). As noted above, the age-depth model was calculated on an event-free depth using a smooth spline with the "clam" R-code package (Blaauw, 2010). This revealed that the sequence FOR covers the last millennium with a mean sedimentation rate of 1 mm yr^{-1} (without the event layers).

5 Discussion

5.1 Different triggers for the event layers

5.1.1 Mass movements

The unusual presence of gravel and aquatic plant remains, in combination with the chaotic sedimentary structures and the localized deposition areas, suggest that the coarse-grained layers correspond to debrites, i.e. deposits resulting from debris flows originating from sediment-charged slopes (e.g. Sauerbrey et al., 2013). The three turbidites overlying the debrites are then interpreted as mass-movement-induced turbidites (MMIT), i.e. resulting from the sediment that is transported in suspension during sliding of slope sediments and then deposited over the debrites and further into the lake basin (e.g. Girardclos et al., 2007; Moernaut et al., 2014). These MMITs are well characterized by higher Ca contents that suggest a distinctly different sediment source when compared to the sedimentary background and to the other turbidites. The debrite associated to MMIT3 is only present in core FOR13P3, suggesting a littoral origin of the mass movement (Fig. 2). The two other debrites (associated to MMIT1 and MMIT2) are located in core FOR13P4 (Fig. 2). These related mass movement deposits may thus originate either from the delta or from the littoral slopes. Slope angles of $< 10^{\circ}$ and $\sim 15^{\circ}$ for delta and littoral slopes, respectively, point to a littoral origin (e.g. Moernaut et al., 2007; Strasser et al., 2011; Van Daele et al., 2013). In addition, higher

CPD
11, 4943–4984, 2015

Ca contents are often a feature of littoral sediments as a result of increased fluxes of endogenic calcite when compared to the open-water endogenic production.

5.1.2 Flood events

Turbidites may be induced by either mass movements or flood events (e.g. Sturm and Matter, 1978). Due to their position directly overlaying the debrites, the three thick turbidites labelled MMIT in Fig. 2 clearly result from mass-movement processes. For the other 168 turbidites, their extents over the whole basin with a relatively homogeneous deposition pattern, their frequent occurrence and a different geochemical pattern suggest a distinct origin. The low Ca contents suggest a minor sediment contribution of the marble and calc-schists in favour of a major contribution of the arkose band, which is the lithology drained by the main inflow (Fig. 1). The 168 turbidites are also characterized by sharp peaks of Mn only located at their bases. This location suggests that the punctual enrichement in Mn is related to the occurrence of these event layers. Mn is a redox sensitive element and more soluble under reducing conditions (e.g. Davison, 1993; Torres et al., 2014). The punctual presence of detectable Mn at the base of the turbidites suggests that hyperpycnal turbidity currents carry oxygen to the deeper parts of the basin. Dissolved oxygen is probably also trapped in pore waters of the individual turbidite deposits. Based on these considerations we suggest that dissolved and reduced Mn is, in part due to the rapid increase in loading from the flood turbidite, migrating from pore waters of the buried sediments into oxygenated turbidite deposts where it is oxidized and precipitated likely in form of an oxyhydroxide (e.g. Davison, 1993; Deflandre et al., 2002). The fast sediment deposition during the event-layer formation and the low reactive organic matter concentrations would then prevent reductive dissolution of the Mn-oxyhydrxide precipitates (e.g. Torres et al., 2014). According to the turbidite characteristics, flood events are the most probable candidate to trigger them because (i) these events may be frequent (e.g. Czymzik et al., 2013), (ii) these events may bring both high oxgygen and detrital inputs in a short time (e.g. Deflandre et al., 2002), and (iii) the nature of the sediment correspond the most to the main lithol-

CPD
11, 4943–4984, 2015

Frequency and intensity of palaeofloods

B. Wilhelm et al.

ogy drained by the inflow. Hence, the 168 turbidites likely correspond to flood-induced turbidites (FIT).

5.1.3 Chronological controls

Mass-movement deposits can be triggered by spontaneous failures due to overloading/oversteepening of sediments-charged slopes, snow avalanches, rockfalls, earthquakes or fluctuations in lake levels (e.g. Monecke et al., 2004; Girardclos et al., 2007; Moernaut et al., 2014). In case of Lake Foréant, changes in lake level can be excluded because water levels of Lake Foréant are well controlled by bedrock outlets. In addition, there is no geomorphological evidence of major rockfalls in the catchment area. Regarding earthquakes, many events occurred in the region and affected the population and infrastructure. Historical earthquakes are well documented thanks to the database SisFrance (http://www.sisfrance.net, Lambert and Levret-Albaret, 1996; Scotti et al., 2004). An earthquake trigger for the mass-movement deposits can then be investigated by comparing ages of the mass-movement deposits to the dates of the closest and/or strongest historical earthquakes (e.g. Avşar et al., 2014; Howarth et al., 2014). The three mass-movement deposits (debrites and their associated MMITs) are respectively dated to AD 1963 (±6), AD 1814 (+50/ – 39) and AD 1456 (+19/ – 56) (Fig. 6). The age of the most recent deposit is consistent with the Saint-Paul-sur-Ubaye earthquake (AD 1959), characterized by an epicentre at ca. 20 km from the lake where the MSK intensity reached VII-VIII. The age of the second deposit is consistent with the Piemont (Torre Pellice) earthquake (AD 1808), characterized by an epicentre at ca. 20 km from the lake and a MSK intensity of VIII (Fig. 6). For the older period of the third deposit, only a few earthquakes have been documented in the database, precluding a reliable assignment. The earthquakes of Saint-Paul-sur-Ubaye and Piemont are both the closest and strongest historically-known earthquakes around the lake, suggesting that they are the most probable trigger of the temporarily corresponding subaquatic landslides. Overall, there is a good agreement between major historical events and

CPD
11, 4943–4984, 2015

the calculated ages of the mass-movement deposits supporting their sedimentologic interpretation and the chronology over the last centuries.

5.2 Palaeoflood record

A flood chronicle of the Bouchouse stream was built by dating the 168 FITs over the last millennium. Changes in flood frequency are highlighted through a running sum of flood occurrences with an 11 year (Fig. 7) or 31 year window (Fig. 8). The absence of significant grain-size variability precludes the use of grain size (or related proxy) to assess changes in flood intensity (e.g. Giguet-Covex et al., 2012; Lapointe et al., 2012; Wilhelm et al., 2013, 2015). The relatively homogeneous grain size of the FITs makes the sediment accumulation per event a more suitable proxy of flood intensity (e.g. Jenny et al., 2014). In addition, the relatively homogeneous flood-sediment deposition pattern within the lake basin makes it possible to use the FIT thickness as a proxy of the flood-sediment accumulation (Wilhelm et al., 2012b, 2015; Jenny et al., 2014). Hence, the FIT thickness is here assumed to represent the flood intensity, under the condition that erosion processes and availability of erodible materials in the catchment did not change significantly over time.

5.2.1 Proxy validation

To control the reliability of our reconstruction, the Foréant palaeoflood record is compared to the historical floods at Ristolas located around 8 km downstream the lake (Fig. 1c and Supplement). The almost absence of documented flood event for the Bouchouse stream (outlet of Lake Foréant) precludes an event-to-event comparison (Wilhelm et al., 2015). Hence, the 21 flood events having affected the village of Ristolas and occurring during the ice-free season of the lake (mid-June to mid-November) have been considered to reconstruct a historical flood record (Fig. 7). This includes 6 floods considered as "local" because they only affected the village of Ristolas (catchment area of ca. 80 km^2) and 15 floods considered as "sub-regional" because they also affected other villages downstream (Abriès, Aiguilles, Chateau-Vieille-Ville, catchment area of ~ 320 km^2). Through comparison of the historical chronicles and the lake records, we observe that the ranges of flood-frequency values are similar, i.e. between 0 and around 4 floods per 11 years. We also observe strong similarities in the two flood records with common periods of low flood frequency in AD 1750–1785, 1820–1860 and 1910–1945 and common periods of high flood frequency in AD 1785–1820, AD 1945–1970 and AD 1985–2000. Only a slight time lag (~ 5 years) appears for the latter period in the lake record. Overall, there is then good agreement with the historical data, supporting that Lake Foréant sediments record the variability of past flood events that impacted societies over the last 250 years relatively well. A major inconsistency, however, appears from 1860 to 1910 since numerous floods are documented in the lake record but there is missing evidence for flood in the historical record. A high hydrological activity is documented for the region at this time (e.g. Miramont et al., 1998; Sivan et al., 2010; Wilhelm et al., 2012a, 2015), suggesting that this may result of a historical database locally incomplete.

5.2.2 Potential influences of environmental changes

The Foréant flood record may be considered as relevant over the entire studied period if erosion processes are stable over time. Erosion processes in the catchment-lake system may be affected by modifications in the river-lake system and/or by land-use changes.

The main inflow, the Bouchouse stream, has built a large fluvial plain upstream the lake where it is divided in two main meandering branches. An alternate activity of these branches during floods may disturb the record by triggering variable sediment dispersion within the lake basin (e.g. Wilhelm et al., 2015). However, such processes seem to be unlikely because the stratigraphic correlation highlights a stable pattern of the flood-sediment deposition with the thickest FITs in cores FOR13P2 and FOR13P4 from the depocenter and a thinning of the FIT deposits toward cores FOR13P1 and FOR13P3 located in the slopes (Fig. 2). The fluvial plain may also disturb the record by acting as a sediment trap. Indeed, the meandering river morphology and the gentle slope of the fluvial plain may trigger a decrease of the discharge velocity, resulting in the deposition of the coarser particles on the plain before entering the lake. This may explain the small variability in grain-size in the Foréant sediment record. The grain-size ratio between the base (coarser fraction) and the top (finer fraction) of the FITs is ~ 1.3, while it usually ranges from 5 to 15 in many different geological and environmental settings (e.g. Oslegger et al., 2009; Giguet-Covex et al., 2012; Simmoneau et al., 2013; Wilhelm et al., 2013, 2015; Amman et al., 2015). However, the transport of the finer fraction (up to medium silt) does not seem to be significantly affected as (i) the sedimentation rate of the silty sedimentary background appears relatively stable (Fig. 6) and (ii) the FIT thickness is highly variable over time (Fig. 8).

Erosion processes in the catchment may also be modified by land-use that mainly corresponds at this altitude to changes in grazing pressure. An increase of grazing pressure may make soils more vulnerable to erosion during heavy rainfalls and, thereby, may induce an increased sensitivity of the catchment-lake system to record floods, i.e. higher flood frequency and/or flood-sediment accumulation in the sediment record (e.g. Giguet-Covex et al., 2012). Abundance of *Sporormiella* is assumed to reflect local changes of grazing pressure in Lake Foréant catchment (e.g. Etienne et al., 2013). The concentration of *Sporormiella* ascospores measured in core FOR13P3 oscillated from 5 to 43 cells cm^{-3} through the sequence (Fig. 2), resulting in accumulation rates varying from 12 to 340 cells $cm^2 yr^{-1}$ over time (Fig. 8). This variability in *Sporormiella* abundance has been compared to the variability in flood frequency and flood-sediment accumulation (see Supplement). We do not find significant relationships ($p > 0.05$) between these parameters (Fig. S3 in the Supplement), suggesting that variations in pastoralism seemingly have not had a significant impact on erosion processes in the Foréant catchment. However, two samples covering the period AD 1734–1760 show both high *Sporormiella* accumulation rates and flood frequencies (Fig. 8 and S3). This suggests that the flood frequency during this period may be exacerbated by a punctual and very high grazing pressure. Hence, we postulate that erosion pro-

CPD
11, 4943–4984, 2015

cesses did not change drastically over the studied period, implying that climate is likely the main factor explaining the recorded flood activity, with exception of the period AD 1734–1760.

5.2.3 Palaeoflood activity in the regional climatic setting

Comparison with the historical record shows that the past flood variability is well reproduced by the Foréant record (Fig. 7). The Foréant palaeoflood record is thus interpreted as the recurrence of summer-to-fall flood events triggered by both local and mesoscale convective phenomena. This suggests that flood frequencies and intensities recorded at Foréant result from both Atlantic- and Mediterranean-sourced weather patterns that induce heavy precipitation events at high-altitude. Indeed, Giguet-Covex et al. (2012) and Wilhelm et al. (2012b, 2013) suggested that floods recorded at high altitude in the Atlantic-influenced region of the northern French Alps are mainly triggered by summer local convective events. While Wilhelm et al. (2012a, 2015) suggested that floods recorded at high altitude in the Mediterranean-influenced region of the southern French Alps are mainly triggered by mesoscale convective events.

To discuss the millennium-long flood variability in regard to both Atlantic and Mediterranean climatic influences in the Alpine domain, the Foréant palaeoflood record is compared to the palaeoflood records of Lakes Blanc and Allos (Figs. 7 and 8). Lakes Blanc and Allos have similar characteristics to Lake Foréant such as the high altitude (> 2000 m a.s.l.), the small catchment area (< 3 km^2) and the steep catchment slopes, making possible the comparison. Lake Blanc sediments located in the northern French Alps mainly record Atlantic-sourced weather pattern of high altitude, i.e. summer local convective events (Fig. 1; Wilhelm et al., 2013). In contrast, Lake Allos sediments located in the southern French Alps mainly record Mediterranean-sourced weather patterns of high altitude, i.e. mesoscale convective events (Fig. 1; Wilhelm et al., 2012a, 2015). The last millennium is usually divided in three climatic periods according to the temperature variations; the warm Medieval Climate Anomaly (MCA, ca. AD 950–1250), the cold Little Ice Age (LIA, ca. AD 1300–1900) and the warmer 20th century (e.g.

CPD
11, 4943–4984, 2015

Lamb, 1965; Büntgen et al., 2011; Luterbacher et al., 2012 and references therein). During the MCA, the Foréant flood record shows a low flood frequency with ~ 10 floods per century and, 4 occurrences of thick flood deposits (> 8 mm thick) that we interpret as high-intensity flood events. During the LIA, the Foréant record shows a higher flood frequency with ~ 17 floods per century and only 2 high-intensity events. The 20th century is finally characterized by ~ 17 floods per century and absence of high-intensity events. The increased flood frequency during the long and cold period of the LIA, compared to the MCA, was also observed in the Blanc and Allos records (Wilhelm et al., 2012a, 2013; Fig. 8), as well as in many other records from the European Alps (e.g. Arnaud et al., 2012; Glur et al., 2013; Swierczynski et al., 2013; Wirth et al., 2013a, b; Amann et al., 2015; Schulte et al., 2015) and the north-western Mediterranean area (e.g. Jorda and Provansal, 1996; Camuffo and Enzi, 1995; Jorda et al., 2002; Thorndycraft and Benito, 2006; Moreno et al., 2008; Benito et al., 2008; Arnaud-Fassetta et al., 2010). This common pattern in many flood records of southern Europe may be the result of a southward shift and contemporaneous intensification of the dominant westerly winds during boreal summer related to an increase in the thermal gradient between low (warming) and high (cooling) latitudes (e.g. Bengtsson and Hodges, 2006; Raible et al., 2007). In this scenario, the Alps are likely to experience an increase in precipitation due to the eastward transport of humidity-charged air masses from the Atlantic. In contrary, the occurrence of high-intense floods during both the MCA and the LIA periods is a new feature of regional patterns, since the most intense floods occurred exclusively during the MCA in the Blanc record (Wilhelm et al., 2013) or during the LIA in the Allos record (Wilhelm et al., 2012a; Fig. 8) and other Mediterranean records (Arnaud-Fassetta et al., 2010; Macklin et al., 2010). This suggests that hydro-meteorological processes related to the Atlantic and to the Mediterranean climatic influences may alternatively trigger high intense events in the Foréant area during the MCA and the LIA, respectively. However, the most intense floods at Foréant appear 3 times more frequent during the MCA than during the LIA, a trend that remains true when considering various thickness thresholds (8, 7, 6 or 5 mm) for high-intensity flood events. In addition, the mean sed-

CPD
11, 4943–4984, 2015

iment accumulation per flood event shows values ∼ 50 % higher during the MCA than during the LIA (3.8 vs. 2.4 mm/flood), suggesting an increase of the mean flood-event intensity during the warmer period. These two evidences of increased flood intensity during the warm period may be related to the strengthening of local convective processes due to higher temperatures, as suggested for the north-western flood pattern (Giguet-Covex et al., 2012; Wilhelm et al., 2012b, 2013). In the Foréant area, higher temperatures seem thus to result in a lower flood frequency but in higher flood intensity (expressed as both higher occurrence of high-intensity floods and higher mean event intensity) on the multi-centennial time scale. Flood frequency and intensity during the warmer 20th century, however, do not follow these trends. The frequency is still similar to the LIA one, high-intense events are absent and the mean sediment accumulation per flood event (2.2 mm/flood) is also similar to the LIA. Two hypotheses may be considered to explain this "anomaly". First, this may result from the relatively short period covered by the 20th century (i.e. ∼ 100 years) in comparison with the multi-centennial variability documented for the MCA (i.e. ∼ 300 years) and the LIA (i.e. ∼ 600 years) periods. Thereby, considering stable temperature-flood relationships over time, the 20th century might be a transitional period toward a MCA-like flood pattern with the global warming. This latter possibility would imply an increasing flood hazard in the Foréant region in a near future due to an increased occurrence of high-intensity flood events. Secondly, this may also result from a non-linearity of the flood response to temperature, making the analogy between the MCA and the 20th century more complex, in particular as the current warming is caused by an unprecedendet forcing (greenhouse gases). Moreover, the other external forcing such as solar activity, and volcanic eruptions largely varied over the last millennium (e.g. Servonnat et al., 2010; Delaygue et Bard, 2011; Gao et al., 2012; Crowley and Unterman, 2013) and their non-linear combination also with the greenhouse gases may result in different time-space temperature patterns and, thereby, in different flood responses during these two periods. In order to explore forcing-dependent impacts on the climate–flood relationships, deeper analysis utilizing for example advanced statistics or simulations is required.

CPD
11, 4943–4984, 2015

6 Conclusions

High-resolution sedimentological and geochemical analyses of the Lake Foréant sequence revealed 171 turbidites and 3 debrites. Three of the 171 turbidites show can be differentiated by characteristic geochemical features (high Ca contents and low Mn contents) and by their presence directly above debrites. These turbidites are interpreted as mass-movement-induced turbidites, i.e. resulting from the littoral sediment that is brought into suspension during sliding of slope sediments. The other 168 turbidites show a geochemical pattern similar to the sedimentary background that mainly corresponds to detrital material sourced by the rivers. These turbidites are interpreted as flood-induced turbidites. Only small changes in grain-size variability in the flood-induced turbidites precluded the use of the grain size as a flood-intensity proxy. However, the relatively homogeneous deposition pattern within the lake basin made the flood-deposit thickness a suitable proxy for the reconstruction of flood intensity.

Comparison with local historical data indicates that Foréant sediments sensitively record past flood events with variability in frequency and intensity related to both Atlantic- and Mediterranean-influenced hydro-meteorological processes, i.e. local and mesoscale convective systems occurring from late spring to fall. As there is no evidence of major changes in erosion processes due to landscape evolution or grazing pressure (except maybe for the period AD 1734–1760), we assume that climate and not land-use changes exerts the dominant control on flood variability in the Foréant-record over the past millennium. The comparison to northern and southern flood records, i.e. to Atlantic- and Mediterranean-influenced records, highlights that the increase of flood frequency during the cold period of the LIA is a common feature of all regional flood patterns from the European Alps. The comparison also revealed that high-intensity events in the Foréant region occurred during both the cold LIA and the warm MCA periods. This specific feature of the Foréant flood record likely results from its sensitivity to both Atlantic and Mediterranean climatic influences. However, high-intensity events are more frequent and the flood intensity is higher during the warm MCA. This

CPD
11, 4943–4984, 2015

suggests that flood hazard may increase in the Foréant region in response to global warming. Surprisingly, the flood variability over the warm 20th century appears still similar to the flood variability of the cold LIA period. This 20th century flood trend may be interpreted as the result of a transitional period toward a MCA-like flood pattern. This would imply an increasing flood hazard in the Foréant region in a near future due to more frequent high-intensity flood events. However, this may also result from a non-linear temperature-flood relationship. In order to better understand the underlyning mechanisms deeper analyses employing advanced statistics or simulations need to be applied.

The Supplement related to this article is available online at doi:10.5194/cpd-11-4943-2015-supplement.

Acknowledgements. B. Wilhelm's post-doctoral fellowship (2013–2014) was supported by a grant from the AXA Research Fund. We would also like to thank Pierre Sabatier for his help with analysis of the ^{210}Pb data, Anne-Lise Develle for fruitful discussions, Petra Boltshauser-Kaltenrieder for help with identification of terrestrial-plant remains prior to ^{14}C dating and Nicolas Thouveny and François Demory for providing access to facilities at the CEREGE palaeomagnetic laboratory (Aix-Marseille University) and for fruitful discussions.

References

Amann, B., Sönke, S., and Grosjean, M.: A millennial-long record of warm season precipitation and flood frequency for the North-western Alps inferred from varved lake sediments: implications for the future, Quaternary Sci. Rev., 115, 89–100, 2015.

Appleby, P. G., Richardson, N., and Nolan, P. J.: 241Am dating of lake sediments, Hydrobiologia, 214, 35–42, 1991.

Arnaud, F., Lignier, V., Revel, M., Desmet, M., Pourchet, M., Beck, C., Charlet, F., Trentesaux, A., and Tribovillard, N.: Flood and earthquake disturbance of ^{210}Pb geochronology (Lake Anterne, North French Alps), Terra Nova, 14, 225–232, 2002.

Arnaud, F., Révillon, S., Debret, M., Revel, M., Chapron, E., Jacob, J., Giguex-Covex, C., Poulenard, J., and Magny, M.: Lake Bourget regional erosion patterns reconstruction reveals Holocene NW European Alps soil evolution and paleohydrology, Quaternary Sci. Rev., 51, 81–92, 2012.

Arnaud-Fassetta, G. and Fort, M.: Respective parts of hydroclimatic and anthropic factors in the recent eveolution (1956–2000) of the active channel of the Upper Guil, Queyras, Southern French Alps, Méditerranée, 102, 143–156, 2004.

Arnaud-Fassetta, G., Carcaud, N., Castanet, C., and Salvador, P. G.: Fluviatile palaeoenvironments in archaeological context: geographical position, methodological approach and global change – hydrological risk issues, Quatern. Int., 216, 93–117, 2010.

Avşar, U., Hubert-Ferrari, A., De Batist, M., Lepoint, G., Schmidt, S., and Fagel, N.: Seismically-triggered organic-rich layers in recent sediments from Göllüköy Lake (North Anatolian Fault, Turkey), Quaternary Sci. Rev., 103, 67–80, 2014.

Barletta, F., St-Onge, G., Channell, J. E. T., and Rochon, A.: Dating of Holocene western Canadian Arctic sediments by matching paleomagnetic secular variation to a geomagnetic field model, Quaternary Sci. Rev., 29, 2315–2324, 2010.

Bengtsson, L. and Hodges, K. I.: Storm tracks and climate change, J. Climate, 19, 3518–3543, 2006.

Beniston, M. and Stephenson, D. B.: Extreme climatic events and their evolution under changing climatic conditions, Glob Planet Change, 44,1–9, 2004.

Benito, G., Thorndycraft, V. R., Rico, M., Sanchez-Moya, Y., and Sopena, A.: Palaeoflood and floodplain records from Spain: evidence for long-term climate variability and environmental changes, Geomorphology, 101, 68–77, 2008.

Blaauw, M.: Methods and code for "classical" age modelling of radiocarbon sequences, Quat. Geochronol., 5, 512–518, 2010.

Bloemendal, J., King, J. W., Hall, F. R., and Doh, S.-J.: Rock magnetism of Late Neogene and Pleistocene deep-sea sediments relationship to sediment source, diagenetic processes, and sediment lithology, J. Geophys. Res., 97, 4361–4375, 1992.

Boroneant, C., Plaut, G., Giorgi, F., and Bi, X.: Extreme precipitation over the Maritime Alps and associated weather regimes simulated by a regional climate model: present-day and future climate scenarios, Theor. Appl. Climatol., 86, 81–99, 2006.

Borradaile, G.: Magnetic susceptibility, petrofabrics and strain, Tectonophysics, 156, 1–20, 1988.

CPD
11, 4943–4984, 2015

Boudevillain, B., Argence, S., Claud, C., Ducrocq, V., Joly, B., Lambert, D., Nuissier, O., Plu, M., Ricard, D., Arbogast, P., Berne, A., Chaboureau, J. P., Chapon, B., Crepin, F., Delrieu, G., Doerflinger, E., Funatsu, B. M., Kirstetter, P. E., Masson, F., Maynard, K., Richard, E., Sanchez, E., Terray, L., and Walfpersdorf, A.: Cyclogeneses et precipitations intenses en region mediterraneenne: origines et caracteristiques, La Meteorol., 66, 18–28, 2009.

Büntgen, U., Tegel, W., Nicolussi, K., McCormick, M., Frank, D., Trouet, V., Kaplan, J., Herzig, F., Heussner, U., Wanner, H., Luterbacher, J., and Esper, J.: 2500 years of European climate variability and human susceptibility, Science, 331, 578–582, 2011.

Buzzi, A. and Foschini, L.: Mesoscale meteorological features associated with heavy precipitation in the Southern Alpine Region, Meteorol. Atmos. Phys., 72, 131–146, 2000.

Campbell, C.: Late Holocene lake sedimentology and climate change in southern Alberta, Canada, Quaternary Res., 49, 96–101, 1998.

Camuffo, D. and Enzi, S.: The analysis of two bi-millenary series: Tiber and Po River Floods, in: Climatic Variations and Forcing Mechanisms of the Last 2000 years, NATO ASI Series, Series I: Global Environmental Change, 41, edited by: Jones, P. D. Bradley, R. S., and Jouzel, J., Springer, Stuttgart, 433–450, 1995.

Corella, J. P., Benito, G., Rodriguez-Lloveras, X., Brauer, A., and Valero-Garcès, B. L.: Annually-resolved lake record of extreme hydro-meteorological events since AD 1347 in NE Iberian Peninsula, Quaternary Sci. Rev., 93, 77–90, 2014.

Croudace, I. W., Rindby, A., and Rothwell, R. G.: ITRAX: description and evaluation of a new multi-function X-ray core scanner. in: Rothwell, R. G. (Ed.), New Techniques in Sediment Core Analysis, Geol. Soc. Spec. Publ., 367, 51–63, 2006.

Crowley, T. J. and Unterman, M. B.: Technical details concerning development of a 1200 yr proxy index for global volcanism, Earth Syst. Sci. Data, 5, 187–197, doi:10.5194/essd-5-187-2013, 2013.

Cuven, S., Francus, P., and Lamoureux, S.: Estimation of grain size variability with micro X-ray fluorescence in laminated lacustrine sediments, Cape Bounty, Canadian High Arctic, J. Paleolimnol., 44, 803–817, 2010.

Czymzik, M., Brauer, A., Dulski, P., Plessen, B., Naumann, R., von Grafenstein, U., and Scheffler, R.: Orbital and solar forcing of shifts in Mid- to Late Holocene flood intensity from varved sediments of pre-alpine Lake Ammersee (southern Germany), Quaternary Sci. Rev., 61, 96–110, 2013.

Davis, O. K. and Schafer, D.: *Sporormiella* fungal spores, a palynological means of detecting herbivore density, Palaeogeo., Palaeoclimatol., Palaeoecol., 237, 40–50, 2006.
Davison, W.: Iron and manganese in lakes, Earth-Sci. Rev., 34, 119–163, 1993.
Deflandre, B., Mucci, A., Gagne, J. P., Guignard, C., and Sundby, B.: Early diagenetic processes in coastal marine sediments disturbed by a catastrophic sedimentation event, Geochim. Cosmochim. Ac., 66, 2547–2558, 2002.
Delaygue, G. and Bard, E.: An Antarctic view of Beryllium-10 and solar activity for the past millennium, Clim. Dynam., 36, 2201–2218, 2011.
Donadini, F., M. Korte, and Constable, C. G.: Geomagnetic field for 0–3 ka: 1. New data sets for global modeling, Geochem. Geophy. Geosy., 10, Q06007, doi:10.1029/2008GC002295, 2009.
Durant, Y., Laternser, M., Giraud, G., Etchevers, P., Lesaffre, B., and Merindol, L.: Reanalysis of 44 Yr of Climate in the French Alps (1958–2002): methodology, Model Validation, Climatology, and Trends for Air Temperature and Precipitation, J. Applied Meteorology and Climatology, 48, 429–449, 2009.
Etienne, D. and Jouffroy-Bapicot, I.: Optimal counting limit for fungal spore abundance estimation using *Sporormiella* as a case study, Veget. Hist. Archaeobot, 23, 743–749, 2014.
Etienne, D., Wilhelm, B., Sabatier, P., Reyss, J. L., and Arnaud, F.: Influence of sample location and livestock numbers on *Sporormiella* concentrations and accumulation rates in surface sediments of Lake Allos, French Alps, J. Paleolimnol., 49, 117–127, 2013.
Faegri, K. and Iversen, J.: Textbook of Pollen Analysis, John Wiley and Sons, New York, 328, 1989.
Frei, C., Schöll, R., Fukutome, S., Schmidli, J., and Vidale, P. L.: Future change of precipitation extremes in Europe: intercomparison of scenarios from regional climate models, J. Geophys. Res. Atm., 111, D06105, doi:10.1029/2005JD005965, 2006.
Gao, C., Robock, A., and Ammann, C.: Volcanic forcing of climate over the past 1500 years: an improved ice core-based index for climate models, J. Geophys. Res., 113, D23111, doi:10.1029/2008JD010239, 2008.
Giguet-Covex, C., Arnaud, F., Enters, D., Poulenard, J., Millet, L., Francus, P., David, F., Rey, P. J., Wilhelm, B., and Delannoy, J. J.: Frequency and intensity of high altitude floods over the last 3.5 ka in NW European Alps, Quaternary Res., 77, 12–22, 2012.
Gilli, A., Anselmetti, F. S., Glur, L., and Wirth, S. B.: Lake sediments as archives of recurrence rates and intensities of past flood events, in: Dating Torrential Processes on Fans and Cones

– Methods and Their Application for Hazard and Risk Assessment, edited by: Schneuwly-Bollschweiler, M., Stoffel, M., and Rudolf-Miklau, F., Advances of Global Change Research, vol. 47, 225–242, 2012.
Girardclos, S., Schmidt, O. T., Sturm, M., Ariztegui, D., Pugin, A., and Anselmetti, F. S.: The 1996 AD delta collapse and large turbidite in Lake Brienz, Mar. Geol., 24, 137–154, 2007.
Glur, L., Wirth, S. B., Büntgen, U., Gilli, A., Haug, G. H., Schär, C., Beer, J., and Anselmetti, F. S., Frequent floods in the European Alps coincide with cooler periods of the past 2500 years, Sci. Rep., 3, 2770, 2013.
Goldberg, E. D.: Geochronology with 210Pb Radioactive Dating, IAEA, Vienna, 121–131, 1963.
Gottardi, F., Obled, C., Gailhard, J., and Paquet, E.: Statistical reanalysis of precipitation fields based on ground network data and weather patterns: application over French mountains, J. Hydrology, 432–433, 154–167, 2010.
Howarth, J. D., Fitzsimons, S. J., Norris, R. J., and Jacobsen, G. E.: Lake sediments record high intensity shaking that provides insight into the location and rupture length of large earthquakes on the Alpine Fault, New Zealand, Earth Planet. Sc. Lett., 403, 340–351, 2014.
IPCC: The Physical Science Basis. Contribution of Working Group I to the Fifth Assessment Report of the Intergovernmental Panel on Climate Change, edited by: Stocker, T. F., Qin, D., Plattner, G.-K., Tignor, M., Allen, S. K., Boschung, J., Nauels, A., Xia, Y., Bex, V., and Midgley, P. M., Cambridge University Press, Cambridge, UK and New York, NY, USA, 2013.
Jenny, J.-P., Wilhelm, B., Arnaud, F., Sabatier, P., Giguet-Covex, C., Mélo, A., Fanget, B., Malet, E., Ployon, E., and Perga, M. E., A 4D sedimentological approach to reconstructing the flood frequency and intensity of the Rhône River (Lake Bourget, NW European Alps), J. Paleolimnol., 51, 469–483, 2014.
Jorda, M. and Provansal, M.: Impact de l'anthropisation et du climat sur le detritisme en France du sud-est (Alpes du Sud et Provence), B. Soc. Geol. Fr., 167, 159–168, 1996.
Jorda, M., Miramont, C., Rosique, T., and Sivan, O.: Evolution de l'hydrosysteme durancien (Alpes du Sud, France) depuis la fin du Pleniglaciaire superieur, in: Les Fleuves ont une Histoire, Paleo-Environnement des Rivieres et des lacs Francais Depuis 15000 Ans, edited by: Bravard, J.-P. and Magny, M., Errance, Paris, 239–249, 2002.
Korte, M., Donadini, F., and Constable, C. G.: Geomagnetic field for 0–3 ka: 2. A new series of time-varying global models, Geochemistry Geophysics Geosystems (G3), 10, Q06008, doi:10.1029/2008GC002297, 2009.

CPD
11, 4943–4984, 2015

Frequency and intensity of palaeofloods

B. Wilhelm et al.

Title Page
Abstract | Introduction
Conclusions | References
Tables | Figures
◂◂ | ▸▸
◂ | ▸
Back | Close
Full Screen / Esc
Printer-friendly Version
Interactive Discussion

Lamb, H. H.: The early medieval warm epoch and its sequel, Palaeogeogr. Palaeoclimatol. Palaeoecol., 1, 13–37, 1965.
Lambert, J, and Levret-Albaret, A.: Mille ans de séismes en France. Catalogues d'épicentres, paramètres et references, Ouest-Editions, Presses Académiques, Nantes, 1996.
Lionello, P., Abrantes, F., Congedi, L., Dulac, F., Gacic, M., Gomis, D., Goodess, C., Hoff, H., Kutiel, H., Luterbacher, J., Planton, S., Reale, M., Schröder, K., Struglia, M. V., Toreti, A., Tsimplis, M., Ulbrich, U., and Xoplaki, E.: Introduction: Mediterranean Climate: Background Information, in: The Climate of the Mediterranean Region. From the Past to the Future, edited by: Lionello, P., Elsevier (Netherlands), Amsterdam, XXXV–IXXX, 2012.
Lurcock, P. C. and Wilson, G. S.: PuffinPlot: a versatile, user-friendly program for paleomagnetic analysis, Geochem. Geophy. Geosy., 13, Q06Z45, doi:10.1029/2012GC004098, 2012.
Luterbacher, J., García-Herrera, R., Akcer-On, S., Allan, R., Alvarez-Castro, M. C., Benito, G., Booth, J., Büntgen, U., Cagatay, N., Colombaroli, D., Davis, B., Esper, J., Felis, T., Fleitmann, D., Frank, D., Gallego, D., Garcia-Bustamante, E., Glaser, R., González-Rouco, J. F., Goosse, H., Kiefer, T., Macklin, M. G., Manning, S., Montagna, P., Newman, L., Power, M. J., Rath, V., Ribera, P., Riemann, D., Roberts, N., Sicre, M., Silenzi, S., Tinner, W., Valero-Garces, B., van der Schrier, G., Tzedakis, C., Vannière, B., Vogt, S., Wanner, H., Werner, J. P., Willett, G., Williams, M. H., Xoplaki, E., Zerefos, C. S., and Zorita, E.: A review of 2000 years of paleoclimatic evidence in the Mediterranean, in: The Climate of the Mediterranean region: From the Past to the Future, edited by: Lionello, P., Elsevier, Amsterdam, the Netherlands, 87–185, 2012.
Macklin, M. G., Tooth, S., Brewer, P. A., Noble, P. L., and Duller, G. A. T.: Holocene flooding and river development in a Mediterranean steepland catchment: the Anapodaris Gorge, south-central Crete, Greece, Global Planet. Change, 70, 35–52, 2010.
Miramont, C., Jorda, M., and Pichard, G.: Évolution historique de la morphogenèse et de la dynamique fluviale d'une rivière méditerranéenne: l'exemple de la moyenne durance (France du sud-est), Géogr. Phys. Quatern., 52, 381–392, 1998.
Moernaut, J., De Batist, M., Charlet, F., Heirman, K., Chapron, E., Pino, M., Brümmer, R., and Urrutia, R.: Giant earthquakes in South-Central Chile revealed by Holocene mass-wasting events in Lake Puyehue, Sediment. Geol., 195, 239–256, 2007.
Moernaut, J., Van Daele, M., Heirman, K., Fontijn, K., Strasser, M., Pino, M., Urrutia, R., and De Batist, M.: Lacustrine turbidites as a tool for quantitative earthquake reconstruction: new

evidence for a variable rupture mode in south central Chile, J. Geophys. Res. Solid Earth, 119, 1607–1633, doi:10.1002/2013JB010738, 2014.
Monecke, K., Anselmetti, F. S., Becker, A., Sturm, M., and Giardini, D.: The record of historic earthquakes in lake sediments of Central Switzerlanc, Tectonophysics, 394, 21–40, 2004.
Moreno, A., Valero-Garces, B. L., Gonzalez-Samperiz, P., and Rico, M.: Flood response to rainfall variability during the last 2000 years inferred from the Taravilla Lake record (Central Iberian Range, Spain), J. Palaeolimnol., 40, 943–961, 2008.
Munich Re Group: Annual Review: Natural Catastrophes 2002, Munich Re Group, Munich, Germany, 2003.
Noren, A. J., Bierman, P. R., Steig, E. J., Lini, A., and Southon, J.: Millennial-scale storminess variability in the northeastern United States during the Holocene epoch, Nature, 419, 821–824, 2002.
Oslegger, D. A., Heyvaert, A. C., Stoner, J. S., and Verosub, K. L.: Lacustrine turbidites as indicators of Holocene storminess and climate: Lake Tahoe, California and Nevada, J. Paleolimnol., 42, 103–122, 2009.
Parajka, J., Kohnová, S., Bálint, G., Barbuc, M., Borga, M., Claps, P., Cheval, S., Dumitrescu, A., Gaume, E., Hlavčová, K., Merz, R., Pfaundler, M., Stancalie, G., Szolgay, J., and Blöschl, G.: Seasonal characteristics of flood regimes across the Alpine–Carpathian range, J. Hydrol., 394, 78–89, 2010.
Passega, R.: Grain-size representation by CM patterns as a geological tool, J. of Sedimentary Petrology, 34, 830–847, 1964.
Plaut, G., Schuepbach, E., and Doctor, M. Heavy precipitation events over a few Alpine subregions and the links with large-scale circulation, 1971–1995, Clim. Res., 17, 285–302, 2009.
Raible, C. C., Yoshimori, M., Stocker, T. F., and Casty, C.: Extreme midlatitude cyclones and their implications for precipitation and wind speed extremes in simulations of the Maunder Minimum versus present day conditions, Clim. Dynam., 28, 409–423, 2007.
Rajczak, J., Pall, P., and Schär, C.: Projections of extreme precipitation events in regional climate simulations for Europe and the Alpine Region, J. Geophys. Res. Atm., 118, 1–17, 2013.
Reimer, P. J., Bard, E., Bayliss, A., Beck, J. W., Blackwell, P. G., Bronk Ramsey, C., Buck, C. E., Cheng, H., Edwards, R. L., Friedrich, M., Grootes, P. M., Guilderson, T. P., Haflidason, H., Hajdas, I., Hatt, C., Heaton, T. J., Hogg, A. G., Hughen, K. A., Kaiser, K. F., Kromer, B., Manning, S. W., Niu, M., Reimer, R. W., Richards, D. A., Scott, E. M., Southon, J. R., Tur-

CPD
11, 4943–4984, 2015

Frequency and intensity of palaeofloods

B. Wilhelm et al.

ney, C. S. M., and van der Plicht, J.: IntCal13 and MARINE13 radiocarbon age calibration curves 0–50000 years calBP, Radiocarbon, 55, 1869–1887, 2013.
Rochette, P., Jackson, M., and Aubourg, C.: Rock magnetism and the interpretation of anisotropy of magnetic susceptibility, Rev. Geophys., 30, 209–226, 1992.
Rochette, P., Vadeboin, F., and Clochard, L.: Rock magnetic applications of Halbach cylinders, Phys. Earth Planet. In., 126, 109–117, 2001.
Sauerbrey, M. A., Juschus, O., Gebhardt, A. C., Wennrich, V., Nowaczyk, N. R., and Melles, M.: Mass movement deposits in the 3.6 Ma sediment record of Lake El'gygytgyn, Far East Russian Arctic, Clim. Past, 9, 1949–1967, doi:10.5194/cp-9-1949-2013, 2013.
Schulte, L., Peña, J. C., Carvalho, F., Schmidt, T., Julià, R., Llorca, J., and Veit, H.: A 2600-year history of floods in the Bernese Alps, Switzerland: frequencies, mechanisms and climate forcing, Hydrol. Earth Syst. Sci., 19, 3047–3072, doi:10.5194/hess-19-3047-2015, 2015.
Schwartz, S., Tricart, P., Lardeaux, J. M., Guillot, S., and Vidal, O.: Late tectonic and metamorphic evolution of the Piedmont accretionary wedge(Queyras Schistes lustrés, western Alps): evidences for tilting during Alpine collision, Geol. Soc. Ame. Bull., 121, 502–518, 2009.
Scotti, O., Baumont, D., Quenet, G., and Levret, A.: The French macroseismic database SISFRANCE: objectives, results and perspectives, Annals of Geophysics, 47, 571–581, 2004.
Servonnat, J., Yiou, P., Khodri, M., Swingedouw, D., and Denvil, S.: Influence of solar variability, CO_2 and orbital forcing between 1000 and 1850 AD in the IPSLCM4 model, Clim. Past, 6, 445–460, doi:10.5194/cp-6-445-2010, 2010.
Simonneau, A., Chapron, E., Vannière, B., Wirth, S. B., Gilli, A., Di Giovanni, C., Anselmetti, F. S., Desmet, M., and Magny, M.: Mass-movement and flood-induced deposits in Lake Ledro, southern Alps, Italy: implications for Holocene palaeohydrology and natural hazards, Clim. Past, 9, 825–840, doi:10.5194/cp-9-825-2013, 2013.
Sivan, O., Miramont, C., Pichard, G., and Prosper-Laget, V.: Les conditions climatiques de la torrentialité au cours du Petit Age Glaciaire de Provence, Archeologie du Midi Medieval, 26, 157–168, 2009.
Stockmarr, J.: Tablets with spores used in absolute pollen analysis, Pollen Spores, 13, 615–621, 1971.
Støren, E. N., Olaf Dahl, S., Nesje, A., and Paasche Ø.: Identifying the sedimentary imprint of high-frequency Holocene river floods in lake sediments: development and application of a new method, Quaternary Sci. Rev., 29, 3021–3033, 2010.

CPD
11, 4943–4984, 2015
Frequency and intensity of palaeofloods
B. Wilhelm et al.

Strasser, M., Hilbe, M., and Anselmetti, F. S.: Mapping basin-wide subaquatic slope failure susceptibility as a tool to assess regional seismic and tsunami hazards, Mar. Geophys. Res., 32, 331–347, 2011.

Sturm, M. and Matter, A.: Turbidites and varves in Lake Brienz (Switzerland): deposition of clastic detritus by density currents, Int. Assoc. Sedimentol. Spec. Publ., 2, 147–168, 1978.

Swierczynski, T., Lauterbach, S., Dulski, P., Delgado, J., Merz, B., and Brauer, A.: Mid- to late Holocene flood frequency changes in the northeastern Alps as recorded in varved sediments of Lake Mondsee (Upper Austria), Quaternary Sci. Rev., 80, 78–90, 2013.

Tachikawa, K., Cartapanis, O., Vidal, L., Beaufort, L., Barlyaeva, T., and Bard, E.: The precession phase of hydrological variability in the Western Pacific Warm Pool during the past 400 ka, Quaternary Sci. Rev., 30, 3716–3727, 2011.

Tarling, D. H. and Hrouda, F.: The Magnetic Anisotropy of Rocks, Chapman and Hall, London, 218 pp., 1993.

Thorndycraft, V. R. and Benito, G.: Late Holocene fluvial chronology of Spain: the role of climatic variability and human impact, Catena, 66, 34–41, 2006.

Torres, N. T., Och, L. M., Hauser, P. C., Furrer, G., Brandl, H., Vologina, E., Sturm, M., Bürgmann, H., and Müller, B.: Early diagenetic processes generate iron and manganese oxide layers in the sediments of Lake Baikal, Siberia, Env. Sci.: Processes Impacts, 16, 879–889, 2014.

Van Daele, M., Versteeg, W., Pino, M., Urrutia, R., and De Batist, M.: Widespread deformation of basin-plain sediments in Aysén fjord [Chile] due to impact by earthquake-triggered, onshore-generated mass movements, Marine Geol., 337, 67–79, 2013.

Van Geel, B. and Aptroot, A.: Fossil ascomycetes in Quaternary deposits, Nova Hedwig, 82, 313–329, 2006.

Van Geel, B., Buurman, J., Brinkkemper, O., Schelvis, J., Aptroot, A., van Reenen, G., and Hakjbilj, T.: Environmental reconstruction of a Roman period settlement site in Uitgeest (the Netherlands), with special reference to coprophilous fungi, J. Archaeol. Sci., 30, 873–883, 2003.

Wilhelm, B., Arnaud, F., Sabatier, P., Crouzet, C., Brisset, E., Chaumillon, E., Disnar, J. R., Guiter, F., Malet, E., Reyss, J. L., Tachikawa, K., Bard, E., and Delannoy, J. J.: 1400 years of extreme precipitation patterns over the Mediterranean French Alps and possible forcing mechanisms, Quaternary Res., 78, 1–12, 2012a.

Wilhelm, B., Arnaud, F., Enters, D., Allignol, F., Legaz, A., Magand, O., Revillon, S., Giguet-Covex, C., and Malet, E.: Does global warming favour the occurrence of extreme floods in European Alps? First evidences from a NW Alps proglacial lake sediment record, Clim. Change, 113, 563–581, 2012b.

Wilhelm, B., Arnaud, F., Sabatier, P., Magand, O., Chapron, E., Courp, T., Tachikawa, K., Fanget, B., Malet, E., Pignol, C., Bard, E., and Delannoy, J. J.: Palaeoflood activity and climate change over the last 1400 years recorded by lake sediments in the NW European Alps, J. Quat. Sci., 28, 189–199, 2013.

Wilhelm, B., Sabatier, P., and Arnaud, F.: Is a regional flood signal reproducible from lake sediments?, Sedimentology, 62, 1103–1117. 2015.

Wirth, S. B., Glur, L., Gilli, A., and Anselmetti, F. S.: Holocene flood frequency across the Central Alps – solar forcing and evidence for variations in North Atlantic atmospheric circulation, Quaternary Sci. Rev., 80, 112–128, 2013a.

Wirth, S. B., Gilli, A., Simonneau, A., Ariztegui, D., Vannière, B., Glur, L., Chapron, E., Magny, M., and Anselmetti, F. S.: A 2000-year long seasonal record of floods in the southern European Alps, Geophys. Res. Let., 40, 4025–4029, 2013b.

CPD
11, 4943–4984, 2015

CPD
11, 4943–4984, 2015

Table 1. Radiocarbon dates of core FOR13P4. We calculated the event-free sedimentary depth by removing the graded beds, which were considered to be instantaneous deposits. See text for explanation, nature of samples and calibration procedures.

BE nr.	Core	Core depth (cm)	Core depth in core FOR13P2 (cm)	Event-free depth in core FOR13P2 (cm)	Material	^{14}C yrs. BP	Cal. yrs BP ($\pm 2\sigma$)	Cal. yrs AD ($\pm 2\sigma$)
2094.1.1	FOR13P4	84–85	82–83	33	Terrestrial	650 ± 18	561–665	1285–1389
2095.1.1	FOR13P4	109–111	106–108	46 ± 0.5	plant	1052 ± 33	923–1052	898–1027
2096.1.1	FOR13P4	113–115	110–112	47 ± 0.5	remains	1242 ± 66	1004–1292	658–946

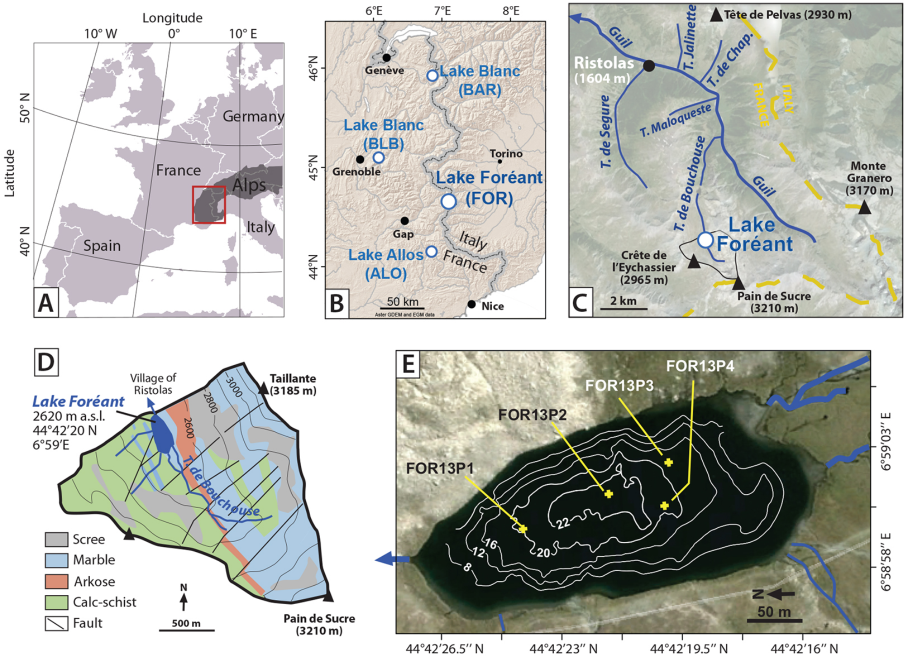

Figure 1. (a) Location of Lake Foréant in the Western Alps, **(b)** compared to the locations of the previously studied Lakes Blanc (BLB, Wilhelm et al., 2012b; BAR, Wilhelm et al., 2013) and Lake Allos (ALO, Wilhelm et al., 2012a). **(c)** Location of the Foréant catchment area in the hydrological network flowing to the village of Ristolas. **(d)** Geological and geomorphological characteristics of the Foréant catchment area. **(e)** Bathymetric map of Lake Foréant and coring sites.

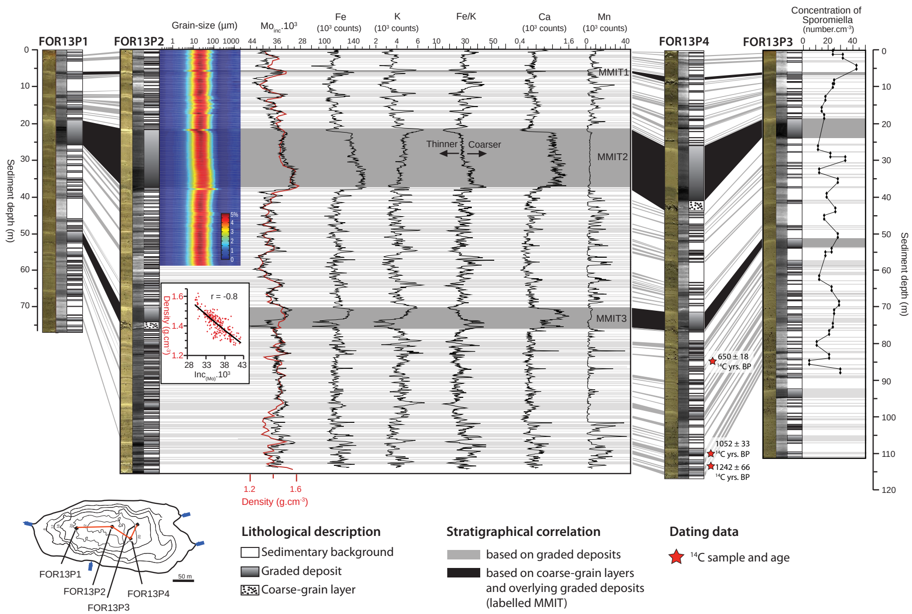

Figure 2. Lithological descriptions of cores and stratigraphic correlations based on sedimentary facies. For each core, a photography (left), a X-ray image (center) and a stratigraphic log is shown (right). ^{14}C samples are indicated by red stars. Variability in grain-size distribution and geochemical elements (Fe, K, Ca and Mn) is shown for the core FOR13P2. Mo_{inc} used as a high-resolution proxy of density is shown close to the density measurements performed by gamma-ray attenuation. Variability in Sporomiella concentration is shown for core FOR13P3.

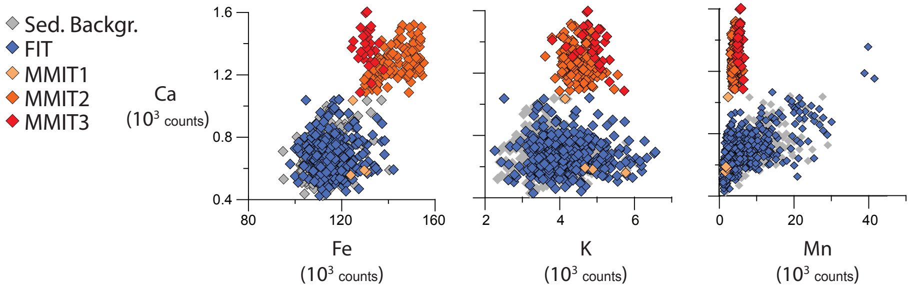

Figure 3. Ca contents plotted against Fe, K and Mn contents for the different lithofacies. FIT refers to flood- and MMIT to mass-movement-induced turbidites. The different MMITs are labelled according to Fig. 2.

CPD
11, 4943–4984, 2015

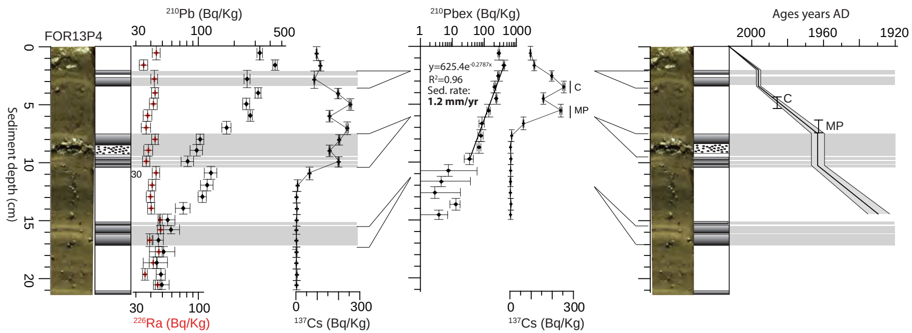

Figure 4. (a) ^{226}Ra, ^{210}Pb and ^{137}Cs profiles for core ALO09P12. **(b)** Application of a CFCS model to the event-free sedimentary profile of ^{210}Pb in excess (without the thick graded beds considered as instantaneous deposits). **(c)** Resulting age–depth relationship with 1σ uncertainties and locations of the historic ^{137}Cs peaks supporting the ^{210}Pb-based ages. C corresponds to the historic ^{137}Cs peak of Chernobyl (AD 1986) and MP to the maximum ^{137}Cs peak of the nuclear fallout (AD 1963).

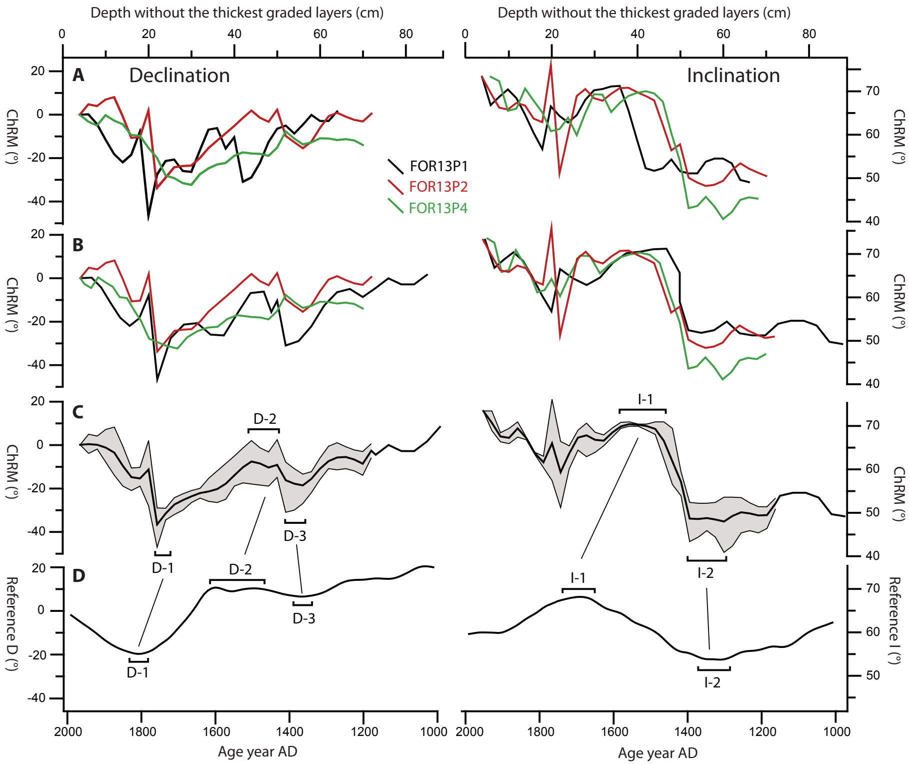

Figure 5. (a) Raw declination and inclination profiles of cores FOR13P1, FOR13P2 and FOR13P4. **(b)** The same profiles after removal of the thickest graded beds (interpreted as event layers) and adjustment of the different specific-core depths to a common reference depth. **(c)** Average of profiles shown in **(b)**. **(d)** Correlation to the ARCH3.4k model reference curve of declination and inclination (Donadini et al., 2009; Korte et al., 2009). ChRM means characteristic remanent magnetization.

CPD
11, 4943–4984, 2015

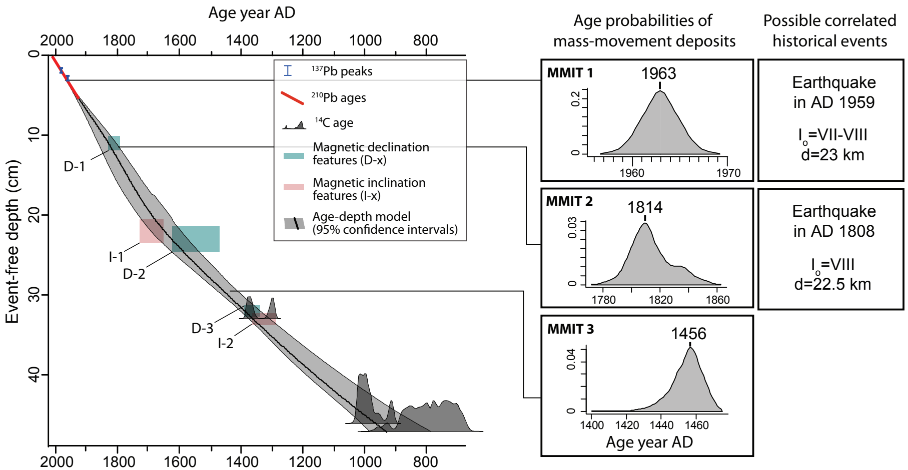

Figure 6. Age–depth model for core FOR13P2 calculated using the "clam" R-code package, combining historic ^{137}Cs peaks, ^{210}Pb ages, calibrated ^{14}C ages and magnetic features on the left side. Probability distribution frequencies of mass-movement ages and possible correlations to historical earthquakes on the right side.

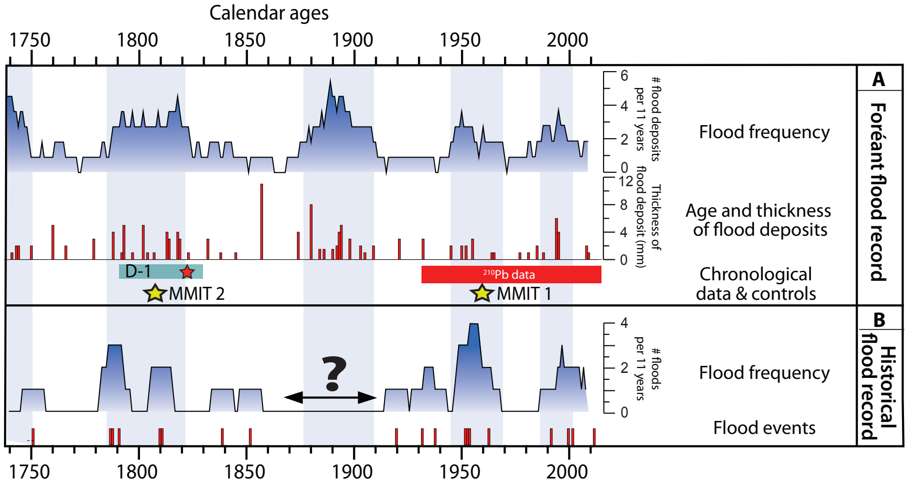

Figure 7. Comparison over the last 250 years of the reconstructed Foréant flood frequency (11 yr running sum) and intensity (thickness of flood deposits) with the frequency (11 yr running sum) of historical floods at Ristolas.

CPD
11, 4943–4984, 2015

Frequency and intensity of palaeofloods

B. Wilhelm et al.

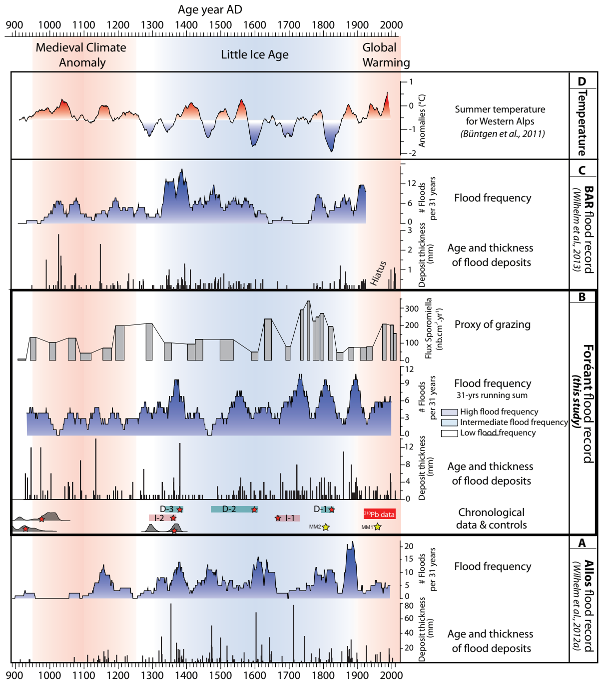

Figure 8. Comparison over the last millennium of **(b)** the reconstructed Foréant flood frequency (31 yr running average) and intensity (thickness of flood deposits) with **(a)** the Allos flood record from the southern French Alps (Wilhelm et al., 2012a), **(c)** the BAR flood record from the northern French Alps (Wilhelm et al., 2013) and **(d)** the tree-ring-based summer temperature for the European Alps (Büntgen et al., 2011). The reconstructed *Sporomiella*-type flux is also shown next to the Foréant flood record to highlight potential human impacts (i.e. grazing) on the erosion processes that might bias the flood record. The red stars below the Foréant record show the chronological markers with their 2 sigma uncertainty ranges.